Pergamon

Int. J. Heat Mass Transfer. Vol. 38, No. 7, pp. 1141–1150, 1995

0017-9310/95 $9.50+0.00

0017-9310(94)00247-9

Experimental study on the crystallization of a binary melt at the vertical boundary of an enclosure

JOSEF TANNY

Center for Technological Education Holon, P.O.B. 305, Holon 58102, Israel

(*Received* 8 *February* 1994 *and in final form* 28 *July* 1994)

Abstract—Crystallization of a uniform binary liquid at the cooled vertical boundary of an enclosure can generate compositional stratification in the melt. During its evolution the induced stratified region is separated from the uniform melt by a sharp density interface which migrates with time. This phenomenon is studied experimentally in an axisymmetric geometry, by cooling and crystallizing a uniform aqueous solution of sodium carbonate (Na_2CO_3) by means of a vertical circular pipe through which coolant is circulated. The investigation is focused on the effect of the applied undercooling on the structure of the crystal and on the growth rates of the stratified layer depth and the typical crystal diameter. It is shown that, at low undercooling, the dendrites at the mush–liquid interface are packed, the stratified layer depth grows as $t^{1.1}$ and the typical crystal diameter grows like $t^{0.45}$ (where t is the time from initiation of cooling). At larger undercooling, the dendrites are spiky and the stratified layer depth and the typical crystal diameter grow like $t^{1.5}$ and $t^{0.7}$, respectively.

1. INTRODUCTION

In recent years a large number of experimental and theoretical studies has been devoted to fluid motions associated with crystallization or solidification processes. In particular, it was recognized that buoyancy and double diffusive heat and mass transfer play important roles due to the coexistence of temperature and concentration gradients in the liquid phase [1, 2].

Among the various configurations studied, considerable attention has been given to the crystallization of an initially uniform binary melt at the vertical boundary of an enclosure [3–6]. Upon crystallization at the vertical boundary, the density of the depleted melt at the vicinity of the growing crystal is decreased (increased) as compared to the ambient and consequently light (heavy) liquid flows towards the top (bottom) of the container.

Turner [3] and Turner and Gustafson [4] have shown experimentally how the above phenomenon can cause the build up of compositional stratification in the melt. If, for example, the depleted liquid is lighter than the ambient, it accumulates at the top of the container, and a sharp density interface separates it from the uniform liquid below. The continuous supply of light liquid to the top of the container, and its interaction with the (initially uniform) environment, gradually build up a stabilizing concentration gradient in the melt. During its evolution, this gradient zone is separated from the uniform melt below by a sharp density front which migrates downwards.

Turner and Gustafson [4] have suggested that the mechanism by which the stratification is established is similar to that of the 'filling box' model of Baines and Turner [7] which predicts the build up of stratification due to the continuous action of a constant buoyancy source in a uniform enclosure. However, Turner and Gustafson [4] have emphasized that in a crystallizing system the simple 'filling box' model is modified in two ways. Firstly, as the crystal grows away from the cooled vertical boundary, its growth rate is reduced as well as the rate of supply of buoyant fluid. This is essentially different from the constant flux of the buoyancy source in the 'filling box' model. Consequently, a state can be achieved at which the rising fluid is unable to penetrate the density interface and hence the downwards migration of the latter ceases at a certain final depth. Secondly, during its generation, the vertical concentration gradient is exposed to a lateral temperature gradient between the solid–liquid interface and the melt. Thus, horizontal double diffusive layers can form by the mechanism also relevant to non-crystallizing double diffusive systems [8–10]. Instead of a smooth concentration profile, as predicted by the 'filling box' model, a 'staircase' structure can be generated.

Using physical and numerical experiments Thompson and Szekely [5, 6] have studied in detail the structure of the melt during the crystallization of aqueous solutions of Na_2CO_3 at the vertical boundary of a cavity. They have shown that horizontal double diffusive layers form within the stratified layer provided a large enough horizontal temperature gradient is maintained between the solid–liquid interface and the ambient melt. For small enough lateral temperature gradient no layering occurred and the stratified zone remained almost stagnant. This phenom-

NOMENCLATURE

c	specific heat
C	concentration
d	cooling pipe diameter
D	typical crystal diameter
h	thickness of stratified layer
H	depth of fluid in the enclosure
K	diffusion coefficient
L	latent heat of fusion
Le	Lewis number, K_t/K_s
m, n	exponents
Pr	Prandtl number, ν/K_t
St	Stefan number, $c(T_L - T_W)/L$
t	time elapsed from initiation of cooling
T	temperature
W	width of enclosure
z	height from the bottom of the enclosure.

Greek symbols

Θ	dimensionless undercooling, $(T_L - T_F)/(T_L - T_E)$
ΔT	undercooling, $T_L - T_F$.

Subscripts

0	ambient
E	eutectic
f	final
F	coolant
L	liquidus
s	solute
t	heat
W	wall.

enon was also observed by Nishimura *et al.* [11] using liquid crystals for temperature field visualization.

The present work was motivated by the observations of Turner and Gustafson [4] that the formation of the gradient zone and its further breakup into a system of horizontal double-diffusive layers have crucial effects on the heat, mass and momentum transports within the melt, and hence on the properties of the crystal formed. As a first step towards the understanding of this problem, we have focused here on the initial stage of the above process, namely, the development of the compositional stratification in an initially uniform binary liquid, cooled and crystallizing at a vertical boundary. In most of the experiments the growth of the solid crystal was also studied. The formation of horizontal double diffusive layers during crystallization is not addressed here; to prevent it we have utilized the above mentioned finding of Thompson and Szekely [5] and insulated the sidewalls of the tank so as to maintain a small enough lateral temperature gradient within the melt (see Section 3).

2. DIMENSIONLESS PARAMETERS

One of the parameters governing crystallization and solidification processes in binary alloys is the Stefan number [12]

$$St = \frac{c(T_L - T_W)}{L} \tag{1}$$

where c is the specific heat of the solid (or the mush, [2]), T_L is the equilibrium liquidus temperature of the initial uniform solution, T_W is the temperature of the cooled boundary and L is the latent heat needed to transform the melt into solid. Thus, St represents the ratio of sensible to latent heat. For a given binary alloy, c and L can be assumed constants, and therefore the undercooling $T_L - T_W$, represents the non-dimensional Stefan number. In the present experiments T_W was not measured directly. Instead we have measured (see Section 3) the coolant temperature at the inlet of the cooling pipe, T_F. Therefore, hereinafter we define the undercooling as $\Delta T = T_L - T_F$.

An important property of a binary alloy is its eutectic temperature T_E. Under equilibrium conditions, in temperatures below the eutectic, both components of the alloy become solid, while above it only one component becomes a solid while the other remains liquid such that a porous mushy zone is formed. As shown below (see Section 4) it is useful to normalize the undercooling using the eutectic temperature of the binary alloy under investigation. Thus we define a dimensionless undercooling as

$$\Theta = \frac{T_L - T_F}{T_L - T_E}. \tag{2}$$

For the binary system Na_2CO_3–H_2O, the eutectic temperature is $T_E = -2.1°C$ [13].

The magnitude of the undercooling determines whether the solid–liquid interface will be spatially planar or irregular during the crystal growth. For large undercooling the crystal grows irregularly and is said to be morphologically unstable [14]. On the other hand, if the undercooling is low enough, the interface is planar, i.e. it is morphologically stable. In the present study the interface seems to be always unstable. However, within the unstable regime, the undercooling controlled the crystal structure and two different morphologies of the dendrites at the mush–liquid (hereinafter denoted as m–l) interface were observed, namely, packed and spiky dendrites (Section 4.2).

During the crystallization process a stage is attained at which the stratified layer growth ceases such that its depth reaches a final value, h_f. The dimensionless final depth is defined here as h_f/H where H, the depth

of the fluid in the enclosure, is the upper limit for the depth of the stratified layer.

Other parameters governing the problem are the aspect ratio of the enclosure H/W where W is the tank width, the dimensionless pipe diameter d/W where d is the cooling pipe diameter, the Prandtl number $Pr = \nu/K_t$ where ν is the kinematic viscosity and K_t is the thermal diffusivity and the Lewis number $Le = K_t/K_s$ where K_s is the solute diffusivity. The values of the latter two parameters, estimated at the concentration and temperature ranges in the experiments [15, 5] are, $Pr = 10.7$ and $Le = 300$.

3. EXPERIMENTAL FACILITIES AND PROCEDURES

The experimental facility is basically similar to the one used by Turner and Gustafson [4]. A square glass tank $20 \times 20 \times 30$ cm high, was fitted with a vertical stainless steel pipe, 8 mm O.D., extending throughout its depth. The resulting dimensionless pipe diameter is $d/W = 0.04$. The sidewalls of the tank were insulated by 4 cm thick plastic insulation plates, which could be removed for observation and photographic purposes. The top and bottom of the tank were insulated by 2.5 cm thick plastic insulation. The solution in the tank was cooled by circulating pre-cooled coolant through the vertical pipe using a constant temperature cooling bath (Haake F3-K).

The crystal growth and the flow patterns were visualized using the shadowgraph technique. The beam of a 35 mW He–Ne laser was filtered and expanded by a spatial filter and then was collimated by a 15 cm diameter plano-convex lens. The resulted parallel circular beam was passed horizontally through the solution and was projected on a semi-transparent paper, attached to the front sidewall of the tank.

Temperatures were measured by thermocouples type T (copper–constantan) using a data acquisition system consisting of a personal computer equipped with A/D and thermocouples boards. The temperatures were measured during the experiment at the inlet and outlet of the cooling pipe, and the vertical distribution of the temperature within the liquid phase was measured by a fixed vertical rake of 12 thermocouples. The rake was located at a radial distance of 5.1 cm from the pipe centerline. The rake thermocouples were calibrated prior to each experiment against the initial uniform temperature of the solution. During calibration the latter temperature was measured independently using a bulb thermometer the accuracy of which was ± 0.2°C. The error in the temperature measurement at the inlet (T_F) and outlet of the cooling pipe is ± 0.5°C. The difference between the measured coolant temperature in the inlet and outlet of the pipe was usually less than 0.7°C. The liquidus temperature for each concentration was estimated using the phase diagram of Na_2CO_3 from ref. [13].

The vertical concentration distribution within the liquid phase was determined by withdrawing small samples (25 μl in volume) of solution at a radial distance of 6 cm from the pipe centerline, and measuring their refractive index by a hand-held salinity refractometer. The refractometer was calibrated at room temperature against three solutions of Na_2CO_3, the concentrations of which cover the range anticipated in the experiment. Each refractive-index measurement was carried out after the withdrawn sample attained the same room temperature. Thus the effect of the variable temperature of the sample on its density was cancelled and the actual concentration could be determined.

Two series of experiments were carried out, each with a different initial concentration and various values of the dimensionless undercooling Θ. The experimental conditions and the main results are listed in Table 1. Series 1 was done with an initial uniform concentration $C_0 = 10.3$ wt % (with one experiment with a slightly smaller $C_0 = 9.85$ wt %) and series 2 was carried out with $C_0 = 12.7$ wt %. In Table 1, n and m are the exponents for the growth of the stratified layer depth and the typical crystal diameter, respectively. Their definitions are given below (see Section 4).

Each experiment started by filling the tank with a uniform solution of sodium carbonate (Na_2CO_3) to a height of 11–11.6 cm. Hence the aspect ratio in all experiments was about $H/W = 0.57$. In most of the experiments the initial uniform temperature of the solution was within the range 16–18°C. Prior to each experiment the solution was allowed to rest for at least 30 min and then, circulation of pre-cooled coolant through the vertical pipe commenced. The coolant temperature was kept constant throughout the experiment. The resulting crystallization process and fluid motions were observed by the shadowgraph technique and photographed by a camera. In particular, the instantaneous depth of the moving front was recorded (see for example the horizontal black lines in Fig. 3(a) below), to study the growth of the compositional gradient layer. As seen in Fig. 3(a) the growing crystal is vertically non-uniform. Therefore we have studied the growth of a typical diameter, which was chosen here as the crystal diameter at the instantaneous level of the moving front.

4. RESULTS AND DISCUSSION

4.1. *The structure of the melt*

The experiments were carried out with solutions of super-eutectic concentration so we expect the depleted liquid to flow upwards and the stratified layer to grow downwards from the top of the container. To identify the density interface separating the stratified layer from the uniform melt below we observe the vertical concentration profile in Fig. 1, measured in a typical experiment with an initial uniform concentration $C_0 = 10.3$ wt % (for which $T_L = 9$°C) and $\Theta = 1.40$.

Table 1. The experimental conditions and results

C_0 [wt %]	ΔT [°C]	Θ	T_0 [°C]	H [mm]	n	m
Series 1						
10.3	9.6	0.87	17.0	115	1.10	0.43
10.3	9.7	0.87	17.0	115	1.10	0.32
10.3	13.4	1.21	16.0	113	1.05	0.44
10.3	15.5	1.40	17.7	112	1.52	0.74
10.3	16.4	1.48	18.0	116	1.47	0.74
9.85	19.0	1.88	14.3	114	1.53	0.65
Series 2						
12.7	9.0	0.60	17.1	113	1.14	0.56
12.7	13.0	0.86	17.0	110	1.15	0.48
12.7	16.0	1.06	17.1	113	1.30	—
12.7	16.5	1.09	16.8	110	1.33	—
12.7	19.0	1.26	17.5	110	1.43	—
12.7	19.5	1.29	16.2	113	1.41	0.67
12.7	23.5	1.56	16.9	114	1.49	0.77
12.7	26.5	1.76	15.4	113	1.58	—

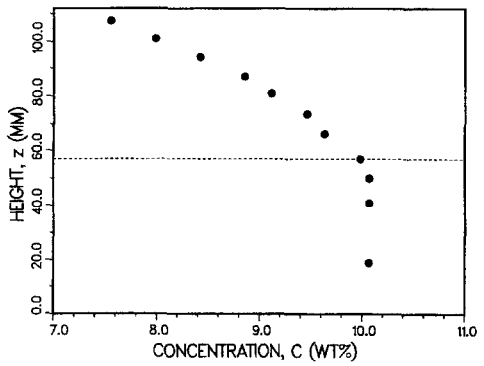

Fig. 1. The vertical concentration profile in the melt (at $t \approx 900$ min) as determined by withdrawing small samples and measuring their refractive index by a refractometer. The dashed horizontal line represents the location of the interface as observed by the shadowgraph technique at $t = 900$ min. The experimental conditions are $C_0 = 10.3$ wt % and $\Theta = 1.4$.

This concentration profile shows that the liquid phase is divided into two different regions: an upper stratified layer with a stabilizing concentration gradient and a lower uniform layer. The horizontal dashed line on this figure (at $z = 57$ mm where z is the height from the bottom of the tank) represents the location of the density interface as observed by the shadowgraph technique at the time the concentration profile was measured. Thus, the front of the stratified layer is identified with the interface observed by the shadowgraph (see e.g. Fig. 3(b) below). All measurements of the stratified layer depth reported below are therefore based on the shadowgraph observations of the moving interface. Concentration profiles similar to that shown in Fig. 1 were also reported by Huppert *et al.* [16] for crystallization at the inclined boundary of an enclosure.

Vertical temperature profiles as measured by the thermocouples rake exhibit the thermal structure of the melt during the crystallization process. Two temperature distributions measured at different times elapsed from the initiation of cooling in an experiment with $C_0 = 10.3$ wt % and $\Theta = 1.40$ are shown in Fig. 2. These profiles illustrate the competition between two physical mechanisms that influence the temperature field as discussed by Turner and Gustafson [4]. Initially, cooling produces a downflow in a cooled and heavier boundary layer adjacent to the pipe surface. This flow induces a stabilizing temperature gradient within the melt as shown by profile *a* in Fig. 2. With time, however, as crystallization progresses, the decrease in concentration more than cancels the density increase due to cooling, so that cooled (but lighter) depleted liquid flows upwards. Consequently, at the upper region of the melt the temperature gradient is reversed and becomes destabilizing, as shown by profile *b* in Fig. 2. Turner and Gustafson [4] suggested that this destabilizing vertical temperature gradient is one of the causes for the formation of horizontal double diffusive layers in the stratified region. In most of our experiments such layers were not observed during the evolution of the stratified region (except for experiments with very low undercooling, see Section 4.2). This implies that the induced

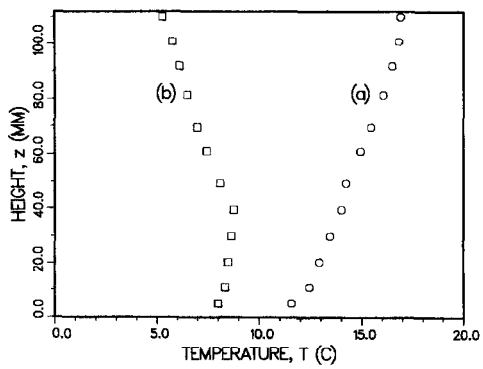

Fig. 2. Two vertical temperature distributions within the melt as measured by the thermocouples rake at different times during the crystallization process. (○) $t = 80$ min, (□) $t = 920$ min. The experimental conditions are $C_0 = 10.3$ wt % and $\Theta = 1.4$.

destabilizing vertical temperature gradient was not large enough to breakup the concentration profile into a series of horizontal layers.

4.2. *The crystal morphology*

In all experiments the observed crystal consisted of a dendritic mushy layer. However, several morphologies and shapes of this mushy zone were observed, depending on the magnitude of the undercooling. The shadowgraphs in Fig. 3 show four typical shapes. We first observe Fig. 3(a) and (b) which illustrates the transition from packed to spiky morphology of the dendrites in two experiments with $C_0 = 10.3$ wt %. In Fig. 3(a) taken from an experiment with $\Theta = 1.21$, we observe a non-planar, irregular m–l interface. We identify the humpy surface of this interface with a packed structure of the dendrites. On the other hand, in an experiment with larger undercooling, $\Theta = 1.40$, the surface of the m–l interface in the stratified zone is much more irregular as shown by the shadowgraph of Fig. 3(b). In particular, at the upper part of the crystal, spiky dendrites are observed which slope down with the distance from the cooling pipe. The shadowgraphs in Fig. 3(a) and (b) were taken at almost the same time ($\approx$900 min) from the initiation of cooling in both experiments. It seems that the increase of about 0.2 in the dimensionless undercooling (which corresponds to an increase of 2.1°C in ΔT) caused a substantial change in the morphology of the m–l interface. In other experiments with the same (or very close to this) initial concentration the above behavior was preserved. In experiments with $\Theta > 1.40$, the m–l interface was spiky while in experiments with $\Theta < 1.21$, the packed structure was observed. These observations suggest that for $C_0 = 10.3$ wt % transition from packed to spiky morphology occurs in the range $1.21 < \Theta < 1.40$.

Spiky crystals similar to those of Fig. 3(b) were observed by Chen and Turner [13] and by Huppert [2] in cooling and crystallizing aqueous solutions of Na_2CO_3 either at a sidewall or at the top of the tank. Chen and Turner [13] suggested that this kind of crystal is formed when the convective motions in the melt are weak, which is in agreement with our observation that spiky crystals develop mainly within the stratified layer, at the upper region of the crystal. This implies that in our experiments with smaller Θ, where spiky crystals do not form, e.g. Fig. 3(a), the convective motion in the upper stratified layer is *stronger* than that in the experiments with larger Θ.

Another series of experiments (series 2 in Table 1) was carried out with a larger initial concentration $C_0 = 12.7$ wt % ($T_L = 13$°C) and various values of the undercooling. Packed and spiky morphologies of the m–l interface were also observed, but the transition from the former to the latter was more gradual than that in series 1 with $C_0 = 10.3$ wt %. For example, the crystal obtained in one experiment of series 2 with $\Theta = 1.06$ is shown in the shadowgraph of Fig. 3(c). It is observed that in this case the m–l interface is more irregular than the packed interface of Fig. 3(a), but it is not as spiky as that in Fig. 3(b). In series 2 a spiky m–l interface was observed for $\Theta \geqslant 1.26$ and a packed interface was found for $\Theta \leqslant 0.86$. This suggests that for $C_0 = 12.7$ wt %, the range of transition from packed to spiky morphology is $0.86 < \Theta < 1.26$.

In the series of experiments with $C_0 = 12.7$ wt %, the value of the dimensionless undercooling at the transition from packed to spiky growth is close to 1. In the series with $C_0 = 10.3$ wt % the transition undercooling is $\Theta \approx 1.3$, somewhat larger than 1. Recalling equation (2) we notice that $\Theta = 1$ when the *coolant* and not the *boundary* temperature is equal to the eutectic temperature. Consequently, for this definition of Θ, we expect $\Theta \geqslant 1$ for a eutectic temperature at the boundary.

We suggest here that in experiments with large Θ the cooled boundary temperature was lower than the eutectic temperature such that a eutectic solid could be formed around the pipe surface. This implies that the spiky mushy crystal observed in Fig. 3(b) surrounds a layer of eutectic solid (which could not be observed). In experiments with lower Θ, apparently no eutectic solid was formed which implies that the packed dendrites seen in Fig. 3(a) occupy the whole crystal. Thus the transition of the m–l interface from the packed to the spiky structure is presumably associated with the decrease of the boundary temperature below the eutectic and the formation of a eutectic solid adjacent to the pipe surface.

When the applied undercooling is much lower a different growth process emerges, as shown in Fig. 3(d) taken from an experiment with $\Theta = 0.4$. During most of this experiment crystallization occurred only at the lower part of the pipe, which resulted in a conical crystal. Only for $t > 900$ min the whole cooling pipe was covered with crystal. Such a conical structure can produce a counter-current flow : an upflow around the region of the growing crystal due to compositional convection and a downflow around the bare upper part of the cooled pipe due to thermal convection. Moreover, in this experiment (and some other experiments performed with a similar Θ), horizontal double-diffusive convection layers were formed within the upper stratified layer. For these two reasons experiments in this low undercooling were excluded from the present study.

4.3. *The growth of the stratified layer*

A typical plot of the stratified layer depth, h, as a function of time taken from an experiment with $C_0 = 10.3$ wt % and $\Theta = 1.21$ is shown in Fig. 4. As seen in the graph, the growth process can be divided into three different stages indicated in Fig. 4 as *a*, *b* and *c*. The first stage *a* in this example is up to about $t = 160$ min at which moment the stratified layer depth is $h = 4$ mm. We identify this stage with the initial transient period during which the melt around the cooling pipe is cooled down to the liquidus tem-

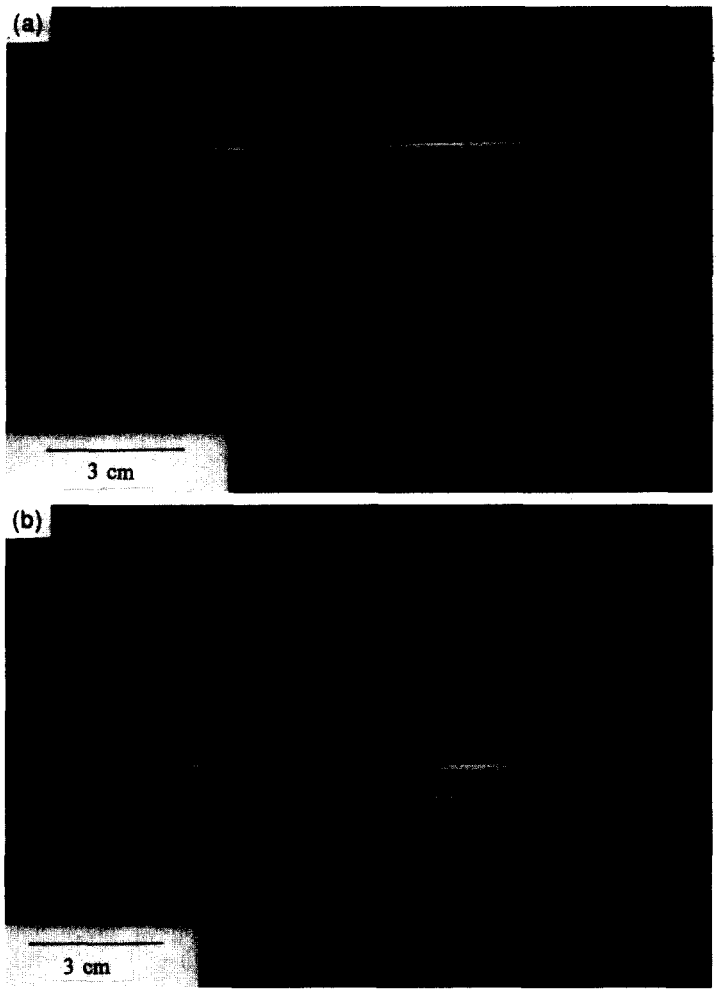

Fig. 3. Some morphologies of the mush/liquid interface. (a) Packed m–l interface, $C_0 = 10.3$ wt %, $\Theta = 1.21$, $t = 905$ min. (The black horizontal lines are marks which represent the location of the density interface at earlier times.) (b) Spiky m–l interface, $C_0 = 10.3$ wt %, $\Theta = 1.4$, $t = 965$ min. (c) Irregular packed structure of the m–l interface, $C_0 = 12.7$ wt %, $\Theta = 1.06$, $t = 857$ min. (d) The conical shape of the crystal at low undercooling, $C_0 = 12.7$ wt %, $\Theta = 0.4$, $t = 670$ min. In all photographs the shadow of the thermocouples rake is seen on the right.

perature and crystallization commences. As crystallization progresses, the migration velocity of the density interface increases as indicated by the larger slope of the data points during stage *b*. Furthermore, it is observed in Fig. 4 that during this stage, this slope is almost constant. In this example stage *b* terminates at about $t = 900$ min at which moment the depth of the stratified layer is $h = 24.5$ mm. During the next stage (*c*) the growth rate of the stratified layer is reduced again and the front seems to approach a final depth of about 35 mm. The latter phenomenon can be explained by the reduced rate of supply of buoyant fluid as discussed in Section 1.

Figure 4 suggests that considerable growth of the stratified layer occurs during stage *b*, where the slope of the data points is almost constant. For this stage, the instantaneous depth of the stratified layer can be expressed as

$$h \propto t^n \tag{3}$$

where n is to be determined experimentally. It must be emphasized that this relation is *not valid* for the *whole* growth process of the stratified layer since, as it is seen in Fig. 4, the layer eventually attains a final depth. Nevertheless, as shown below, this simple power law is useful in characterizing quantitatively the effect of the undercooling on the growth processes observed in these experiments.

In each experiment the value of n was estimated by fitting a straight line to the data points of stage *b* using the least squares method (see Table 1). The time boundaries of stage *b* were chosen such that the maximum standard error in the estimated value of n is 0.04. For most experiments the standard error was less than 0.03. It is noticed that in some experiments the slope of stage *a* was equal to that of stage *b*.

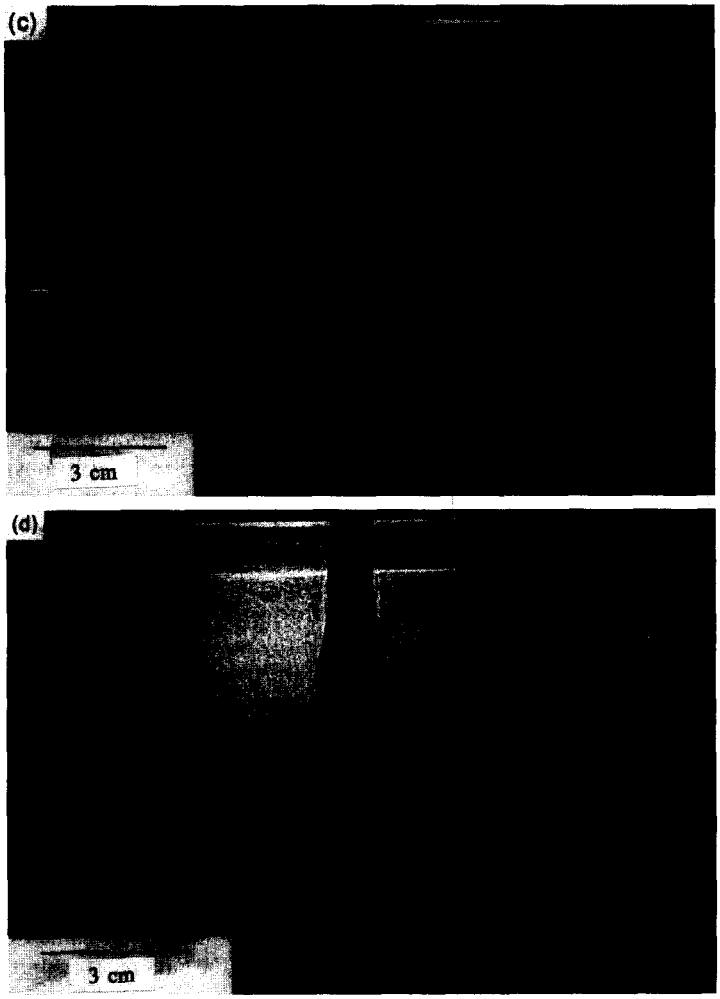

Fig. 3 (*continued*)

Figure 5 shows the values of n as a function of the undercooling Θ for the 14 experiments conducted in this investigation. The results were extracted from the above mentioned (Section 4.2) two series of experiments. The points marked by ● in Fig. 5 are from the series No. 1 with $C_0 = 10.3$ wt % (except for the point $\Theta = 1.88$ with a slightly different $C_0 = 9.85$ wt % and $T_L = 8°C$), while the points marked by □ correspond to the series No. 2 with $C_0 = 12.7$ wt %.

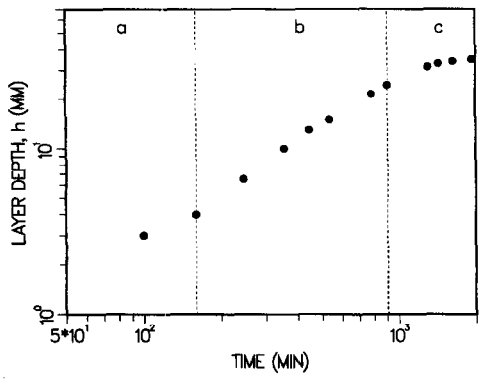

Fig. 4. The depth of the stratified layer developed within the melt, h, as a function of time during crystallization with $C_0 = 10.3$ wt %, $\Theta = 1.21$. a, b and c represent three stages during the growth process.

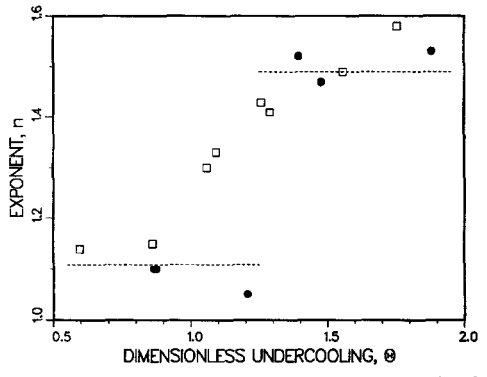

Fig. 5. The exponent n (equation 3) of the growth of the stratified layer depth as a function of the applied undercooling Θ for the two series of experiments: ● – $C_0 = 10.3$ wt %, □ – $C_0 = 12.7$ wt %. The horizontal dashed lines represent the average values of low and high n.

The results of series 1 exhibit essentially two different values of the exponent n, depending on the undercooling (see Table 1). For the three experiments with $\Theta \leqslant 1.21$, the values of n are 1.1, 1.1 and 1.05, while for the three experiments with $\Theta \geqslant 1.40$, the values of n are 1.47, 1.52 and 1.54. In the results of series No. 2 the variation of n with Θ is more gradual than that in series No. 1. For the range of undercooling studied here it seems that n increases linearly with Θ. However, in view of the significant change of the crystal structure at $\Theta \approx 1.1$ (for series No. 2) and the limited range of Θ, we suggest that for this series of experiments the system also assumes regimes of low and high n, with a gradual change from the former to the latter. In particular, for the two experiments with $\Theta \leqslant 0.86$, the values of the exponent n are 1.14, and 1.15 while for the four experiments with $\Theta \geqslant 1.26$, its values are 1.41, 1.43, 1.49 and 1.58. Two experiments of this series with $\Theta = 1.06$ and 1.09 resulted with $n = 1.3$ and 1.33, respectively. Thus, for all experiments mentioned above (excluding the latter two with $n \approx 1.3$), the average value of high n is 1.49 ± 0.06 and the average value of low n is 1.11 ± 0.04. These average values are represented by the dashed lines in Fig. 5. It is noteworthy that for $n > 1$ (during stage b) the growth rate of the stratified layer depth, dh/dt, increases with time.

Recalling the earlier (Section 4.2) observations of the crystal morphology, it is noticed that in each series of experiments, the range of undercooling over which n changes its value corresponds to the transition from packed to spiky growth. Therefore it is suggested that at low undercooling, when the dendrites at the m–l interface are packed the exponent of the growth of the stratified layer depth is 1.1. At larger undercooling, as the dendrites become spiky, the exponent increases to 1.5. Two experiments performed within the range of transition from packed to spiky crystal growth resulted with an intermediate value of $n \approx 1.3$. The irregular packed structure observed in Fig. 3(c) corresponds to one of these experiments.

Very few experimental studies were done in which the growth of the stratified layer due to solidification of aqueous solutions in cavities was analyzed quantitatively. Thompson and Szekely [5] studied two-dimensional crystallization in a sub-eutectic solution with morphologically unstable crystal. On the basis of their observations (their Fig. 2) we have measured the thickness of the stratified layer as a function of time at four states during solidification. These data points resulted with $n = 1.1$ which is very close to our average value of 1.11 for the regime of packed growth in the present axisymmetric geometry. It is noticed that during this experiment they observed horizontal double diffusive layers. Recently, Chellaiah *et al.* [17] studied solidification of NaCl aqueous solution at a vertical boundary. Their initial concentration was sub-eutectic in which case the stratified layer grows from the bottom of the cavity. For one of their experiments they have shown that the thickness of the stratified layer was growing linearly with time. In terms of the present study this means that $n = 1$, which is in fair agreement with our value of 1.11 for the regime of packed growth.

As mentioned earlier, the stratified layer approaches a final depth which must be equal to or smaller than the height of the fluid in the enclosure. The dimensionless final depth of the stratified layer h_f/H was determined in the series of experiments with $C_0 = 10.3$ wt %, and is shown in Fig. 6 as a function of Θ. Regimes of low and high values of h_f/H are observed with a transition at $1.21 < \Theta < 1.40$. The average values of low and high dimensionless depth are 0.23 and 0.70, respectively, and these are represented by the horizontal dashed lines in Fig. 6. In view of our earlier observations of the crystal morphology, it is suggested that the transition from low to high values of h_f/H is associated with the change in the crystal morphology. Thus for a packed m–l interface $h_f/H = 0.23$ while for a spiky interface, $h_f/H = 0.70$.

4.4. *The growth of the crystal*

As seen in Fig. 3 the diameter of the growing crystal is vertically non-uniform mainly because of the environmental stratification. Furthermore, when the m–l interface is spiky its surface is highly irregular as also seen in Fig. 3. Therefore a typical diameter of the crystal was defined as the diameter at the instantaneous depth of the moving density interface.

In Fig. 7 the typical crystal diameter is plotted as a function of time for the same experiment of Fig. 4. Essentially, the data points exhibit a behavior similar to that of the stratified layer depth (Fig. 4), and three different stages are observed. An initial transient period (a), a stage of nearly constant slope (b) and eventually, an approach to a final value (c). Again we focus on stage b during which the growth exponent of the typical crystal diameter seems to be constant. This stage corresponds to stage b of Fig. 4 over which most growth of the stratified layer is taking place. During

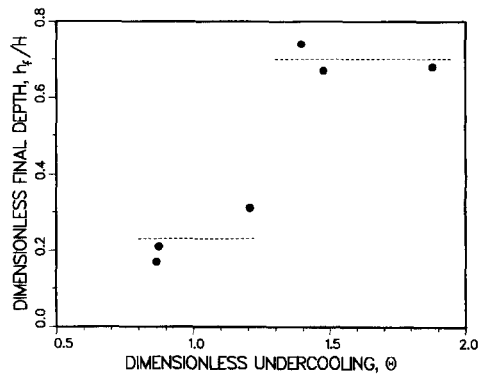

Fig. 6. The dimensionless final depth of the stratified layer h_f/H as a function of the applied undercooling Θ for the series of experiments with $C_0 = 10.3$ wt %. The horizontal dashed lines represent the average values of low and high h_f/H.

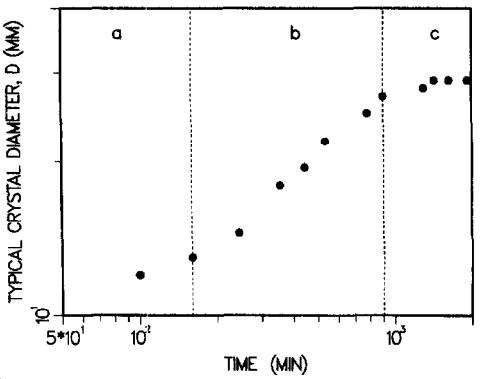

Fig. 7. The typical crystal diameter, D, as a function of time during crystallization with $C_0 = 10.3$ wt %, $\Theta = 1.21$. *a*, *b* and *c* represent three stages during the growth process.

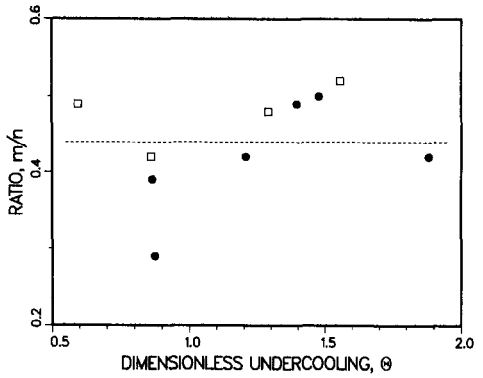

Fig. 9. The ratio m/n as a function of the undercooling Θ. ● $-C_0 = 10.3$ wt %, □ $-C_0 = 12.7$ wt %. The horizontal dashed line represents the average value of m/n.

this stage the instantaneous crystal diameter D can be expressed as

$$D \propto t^m \tag{4}$$

where m is to be determined for each experiment. It is emphasized again that this relation is valid *only* during stage *b* since, as shown in Fig. 7, the crystal eventually approaches a final typical diameter.

In each of the experiments where D was measured, the value of m was estimated by fitting a straight line to the data points corresponding to stage *b*, using the least squares method (see Table 1). The data points of the initial (*a*) and final (*c*) stages were not taken into account. In part of the experiments the growth of the typical crystal diameter with time was highly irregular such that a single value of m could not be determined. The resulted values of m for the two series of experiments with $C_0 = 10.3$ wt % and $C_0 = 12.7$ wt % are shown in Fig. 8 as a function of Θ. The symbols are the same as those in Fig. 5. Two distinct values of m are observed. For high m the average value is $m = 0.71 \pm 0.05$ while for low m, its average value is $m = 0.45 \pm 0.09$. These values are represented by the dashed lines in Fig. 8. The range of undercooling over which m changes its value corresponds to the transition from packed to spiky structure of the m–l interface. Thus, when the m–l interface is packed $m = 0.45$ and when it is spiky $m = 0.7$. In both regimes $m < 1$ (during stage *b*) so that the growth rate of the typical crystal diameter, dD/dt, decreases with time.

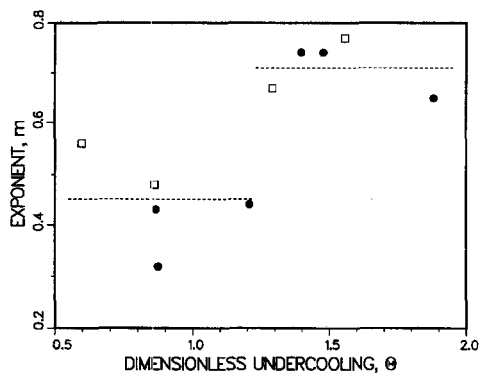

Fig. 8. The exponent m, equation (4), of the growth of the typical crystal diameter as a function of the applied undercooling Θ for the two series of experiments: ● $-C_0 = 10.3$ wt %, □ $-C_0 = 12.7$ wt %. The horizontal dashed lines represent the average values of low and high m.

It is remarkable that $m = 0.45$ for the packed regime, not very different from the $t^{1/2}$ growth associated with one-dimensional (or axisymmetric) crystallization into a semi-infinite domain without convection [2, 18]. On the other hand, when the mush is spiky its growth becomes $t^{0.7}$ which is larger than $t^{1/2}$ for *morphologically unstable* growth in a one-dimensional system [14].

On the basis of the above results, the ratio m/n, which represents the relation between the typical crystal diameter and the stratified layer depth, can be calculated for each experiment. This ratio is shown in Fig. 9 as a function of the dimensionless undercooling. It is seen that m/n is approximately constant, independent of the undercooling and the crystal morphology. The average value of m/n for 10 experiments is 0.44 ± 0.07 (as represented by the dashed line in Fig. 9) which suggests that during stage *b* of the crystallization process, $h \propto D^{2.27}$. This exponent of D is not much different from 2, the exponent anticipated for a linear relation between the instantaneous volumes of the stratified layer and the circular crystal.

5. SUMMARY

The development of a stratified layer due to crystallization of a binary liquid at the outer surface of a vertical circular pipe in an enclosure was investigated experimentally by cooling uniform aqueous solutions of Na_2CO_3. Experiments were carried out at two different initial concentrations and various values of undercooling. The morphology of the m–l interface and the growths of the stratified layer depth and the typical crystal diameter were studied using the shadowgraph technique.

Depending on the value of the dimensionless under-

cooling, two morphologies of the dendrites in the mushy zone were observed: packed and spiky, each associated with a quantitatively different behavior of the system. For a packed m–l interface the stratified layer depth grows like $t^{1.1}$ and the typical crystal diameter like $t^{0.45}$. However, when the m–l interface is spiky the growths of the stratified layer depth and the typical crystal diameter become $t^{1.5}$ and $t^{0.7}$, respectively.

The transition from packed to spiky m–l interface seems to be associated with the decrease of the cooled boundary temperature below the eutectic temperature of the binary solution. In one series of experiments (with $C_0 = 10.3$ wt %) this transition was quite abrupt while in the series with the higher concentration ($C_0 = 12.7$ wt %) it was much more gradual. Thus, further studies both experimental and numerical, are needed to explore the characteristics of this transition process in more detail. Furthermore, before the results obtained here can be applied to geological or industrial solidification processes, more research is required in a wider range of undercooling, in different geometries and aspect ratios of the enclosure and in fluids with different *Pr* and *Le* numbers.

Acknowledgments—The experiments reported here were carried out at the laboratories of the department of mechanics and control at the Center for Technological Education Holon (CTEH). The author is grateful to the executive of the CTEH, and in particular to the Head of the CTEH, Prof. D. Maron for the financial support in the development of the laboratories. The author would like to acknowledge Prof. C. F. Chen for his very useful suggestions. The author would also like to acknowledge Mr S. Shargrotski for the construction of the apparatus.

REFERENCES

1. H. E. Huppert and R. S. J. Sparks, Double-diffusive convection due to crystallization in magmas, *A. Rev. Earth Planet. Sci.* **12,** 11–37 (1984).
2. H. E. Huppert, The fluid mechanics of solidification, *J. Fluid Mech.* **212,** 209–240 (1990).
3. J. S. Turner, A fluid-dynamical model of differentiation and layering in magma chambers, *Nature* **285,** 213–215 (1980).
4. J. S. Turner and L. B. Gustafson, Fluid motions and compositional gradients produced by crystallization or melting at vertical boundaries, *J. Volcanol. Geotherm. Res.* **11,** 93–125 (1981).
5. M. E. Thompson and J. Szekely, Mathematical and physical modelling of double diffusive convection of aqueous solutions crystallizing at a vertical wall, *J. Fluid Mech.* **187,** 409–433 (1988).
6. M. E. Thompson and J. Szekely, Density stratification due to counterbuoyant flow along a vertical crystallization front, *Int. J. Heat Mass Transfer* **32**(6), 1021–1036 (1989).
7. W. D. Baines and J. S. Turner, Turbulent buoyant convection from a source in a confined region, *J. Fluid Mech.* **37,** 51–80 (1969).
8. C. F. Chen, D. G. Briggs and R. A. Wirtz, Stability of thermal convection in a salinity gradient due to lateral heating, *Int. J. Heat Mass Transfer* **14,** 57–65 (1971).
9. H. E. Huppert and J. S. Turner, Ice blocks melting into a salinity gradient, *J. Fluid Mech.* **100,** 367–384 (1980).
10. J. Tanny and A. Tsinober, The dynamics and structure of double diffusive layers in sidewall-heating experiments, *J. Fluid Mech.* **196,** 135–156 (1988).
11. T. Nishimura, M. Fujiwara and H. Miyashita, Visualization of temperature fields and double-diffusive convection using liquid crystals in an aqueous solution crystallizing along a vertical wall, *Exp. Fluids* **12,** 245–250 (1992).
12. J. Crank, *Free- and Moving-Boundary Problems*. Clarendon Press, Oxford (1984).
13. C. F. Chen and J. S. Turner, Crystallization in a double-diffusive system, *J. Geophys. Res.* **85,** 2573–2593 (1980).
14. H. E. Huppert and M. G. Worster, Dynamic solidification of a binary melt, *Nature* **314,** 703–707 (1985).
15. E. W. Washburn, *International Critical Tables of Numerical Data Physics, Chemistry & Technology*, Vol. 5. McGraw-Hill, New York (1929).
16. H. E. Huppert, R. S. J. Sparks, J. R. Wilson and M. A. Hallworth, Cooling and crystallization at an inclined plane, *Earth Planetary Sci. Lett.* **79,** 319–328 (1986).
17. S. Chellaiah, R. A. Waters and M. A. Zampino, Solidification of an aqueous salt solution in the presence of thermosolutal convection, *Warme- und Stoffubertragung* **28,** 205–216 (1993).
18. H. S. Carslaw and J. C. Jaeger, *Conduction of Heat in Solids*, Chap. 11. Clarendon Press, Oxford (1959).